J Mater Sci: Mater Electron (2016) 27:2944–2949
DOI 10.1007/s10854-015-4114-9

Synthesis and characterization of the iron titanate nanoparticles via a green method and its photocatalyst application

Ruhollah Talebi[1] · **Saeid Khademolhoseini**[2] · **Ali Abedini**[3]

Received: 2 September 2015 / Accepted: 20 November 2015 / Published online: 26 November 2015

Abstract Pure iron titanate (Fe_2TiO_5) nanoparticles were successfully synthesized via novel sol–gel method with the aid of $Fe(NO_3)_3{\cdot}9H_2O$, $Ti(OC_4H_9)_4$ (TNBT), and glucose without adding external surfactant. Moreover, glucose plays role as reducing agent, and natural template in the synthesis Fe_2TiO_5 nanoparticles. The structural, morphological and optical properties of as obtained products were characterized by techniques such X-ray diffraction, energy dispersive X-ray microanalysis, scanning electron microscopy, and ultraviolet–visible spectroscopy. The samples indicated a paramagnetic behavior, as evidenced by using vibrating sample magnetometer at room temperature. To evaluate the photocatalyst properties of nanocrystalline iron titanate, the photocatalytic degradation of methyl orange under ultraviolet light irradiation was carried out.

1 Introduction

Materials at the nanometer scale have been studied for decades because of their unique properties arising from the large fraction of atoms residing on the surface, and also from the finite number of atoms in each crystalline core. Especially, because of the increasing need for high area density storage, the synthesis and characterization of semiconductor nanocrystals have been extensively investigated [1–5]. TiO_2 is a commonly used photocatalyst to control aqueous organic contaminates or air pollutants [6–8]. To improve the activity of Fe_2TiO_5 for environmental applications, the absorption of light must be enhanced. If this enhancement were accomplished, Fe_2TiO_5 nanoparticles would offer an attractive option for environmental applications due to its efficient use of sunlight as the source of energy. To further improve the photocatalytic performance, the suitable Fe^{+3} ion concentration for Fe doped TiO_2 showed improved photocatalytic activity than pure TiO_2 because Fe^{+3} can form localized bands near the bottom of conduction band and thereby decreasing band gap [9, 10]. Furthermore, doping with various concentrations of Fe^{+3} enhances electron–hole pair separation by decrease the band gap. The photocatalysis efficiency of TiO_2 can be improved by effectively reducing the electron–hole recombination if Fe_2TiO_5 is formed. So Fe_2TiO_5 plays a very important role on the photocatalytic activity for Fe doped TiO_2 electrically, it is 'n' type of semiconductor [11]. This compound has been investigated extensively for its magnetic spin glass behavior [12, 13]. This compound has short-range antiferromagnetic order, which is partly broken by Ti layers, and the compound has a spin glass transition at 53 K [14]. Recently, the compound has been investigated for its large thermal expansion anisotropy, crystallographic texture, photoelectrode for electrolysis of water, thermodynamic equilibrium, automotive, industrial electronic and food handling and processing and photocatalyst [15–20]. Overall one gets an impression that this compound has the potential of wide range of applications, various chemistry-based processing routes have been developed to synthesize several types of nano sized magnetic particles. There are several methods for synthesis of iron oxide nanocrystals, including ceramic technique and

✉ Ali Abedini
aliabedini074@gmail.com

[1] Young Researchers and Elite Club, Central Tehran Branch, Islamic Azad University, Tehran, Iran

[2] Young Researchers and Elite Club, South Tehran Branch, Islamic Azad University, Tehran, Iran

[3] Young Researchers and Elite Club, Borujerd Branch, Islamic Azad University, Borujerd, Iran

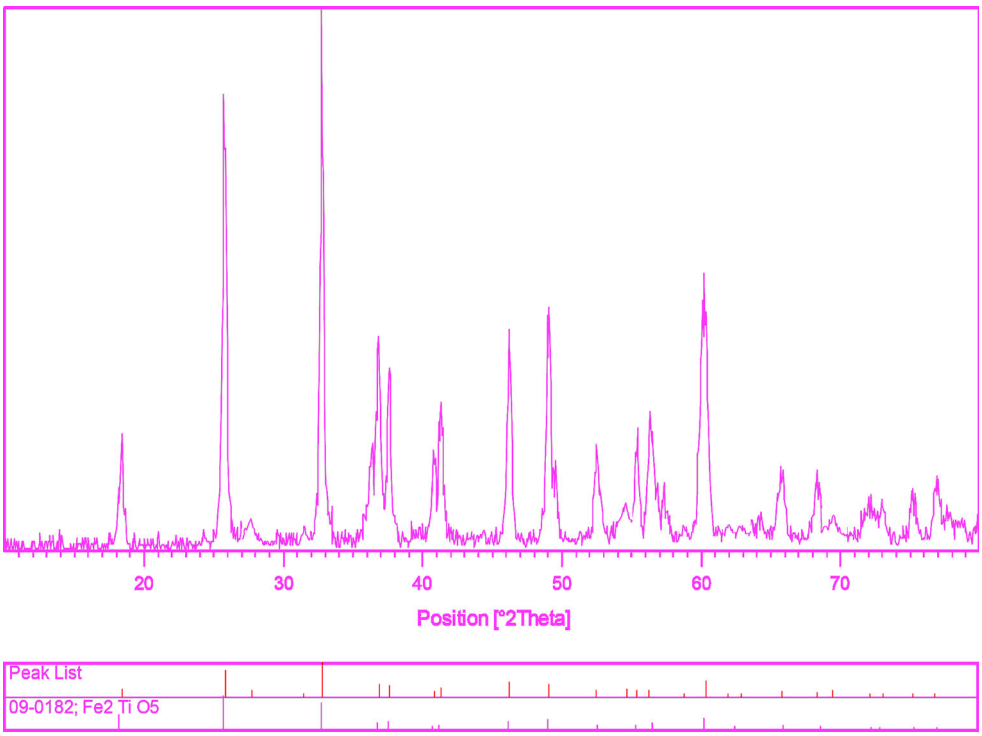

Fig. 1 XRD pattern of Fe_2TiO_5 nanoparticles calcined at 700 °C

solid-state processes which performed in reaction temperature and time above 1000 °C and 20 h [19–22]. In this report, for the first time, we had presented the preparation of Fe_2TiO_5 nanoparticles by novel sol–gel method at 700 °C in the presence of starch without adding external surfactant, capping agent or template. A green approach for Fe_2TiO_5 nanoparticles synthesis by utilizing natural template permits the reaction to proceed usually in milder conditions. Although existing chemical approaches have effectively produced well defined Fe_2TiO_5 nanoparticles, these processes are generally costly and include the employ of toxic chemicals. The photocatalytic degradation was investigated using methyl orange (MO) under ultraviolet light irradiation [23–25].

2 Experimental

2.1 Characterization

X-ray diffraction (XRD) patterns were recorded by a Philips-X'PertPro, X-ray diffractometer using Ni-filtered Cu Kα radiation at scan range of $10 < 2\theta < 80$. The electronic spectra of the cobalt aluminate were obtained on a Scinco UV–vis scanning spectrometer (Model S-10 4100). The energy dispersive spectrometry (EDS) analysis was studied by XL30, Philips microscope. Scanning electron microscopy (SEM) images were obtained on LEO-1455VP equipped with an energy dispersive X-ray spectroscopy. The magnetic measurement of samples were carried out in a vibrating sample magnetometer (VSM) (Meghnatis Daghigh Kavir Co.; Kashan Kavir; Iran) at room temperature.

2.2 Synthesis of Fe_2TiO_5 nanoparticles

All the chemicals used in this method were of analytical grade and used as received without any further purification. At first, 1.1 g of iron (III) nitrate, 1.1 g of glucose, and 0.5 ml acetylacetonate were dissolved in 10 ml distilled ethanol and stirred for 15 min. Then, 1 ml of tetra-n-butyl titanate was added drop wise into solution. After wards, the final mixed solution was kept stirring to form a gel at 90 °C. Finally, the obtained product was placed in a conventional furnace in air atmosphere for 150 min and calcine at 700 °C. After thermal treatment, the system was allowed to cool to room temperature naturally, and the obtained precipitate was collected.

2.3 Photocatalysis experiments

The methyl orange (MO) photodegradation was examined as a model reaction to evaluate the photocatalytic activities of the iron titanate nanoparticles. The photocatalytic experiments were performed under an irradiation ultraviolet light. The photocatalytic activity of nanocrystalline

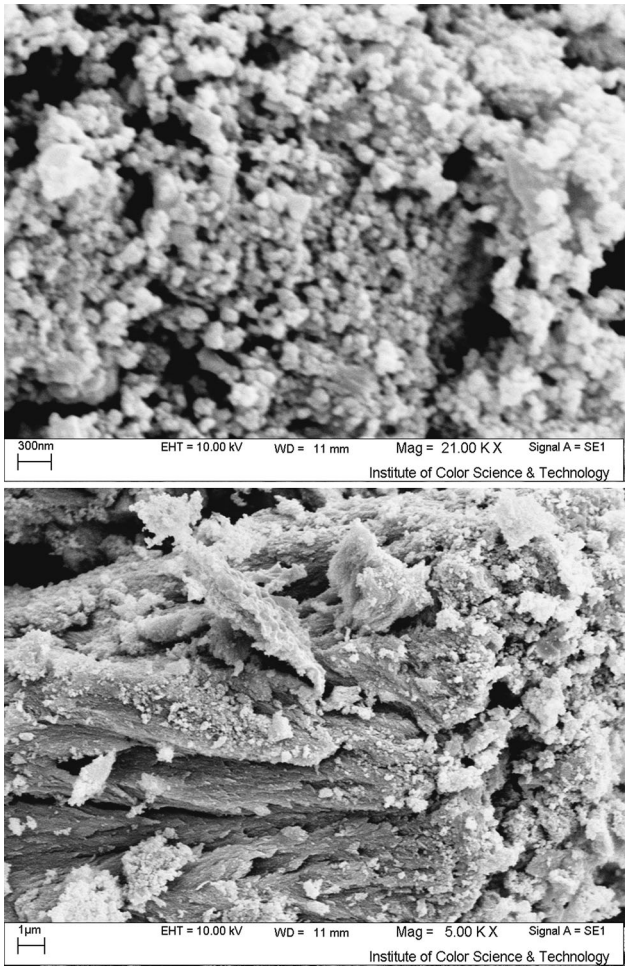

Fig. 2 SEM image of Fe_2TiO_5 nanoparticles calcined at 700 °C

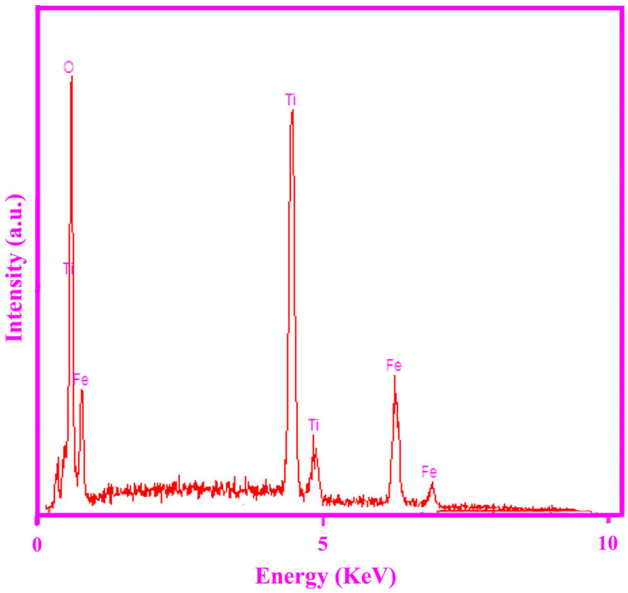

Fig. 3 EDS pattern of Fe_2TiO_5 nanoparticles calcined at 700 °C

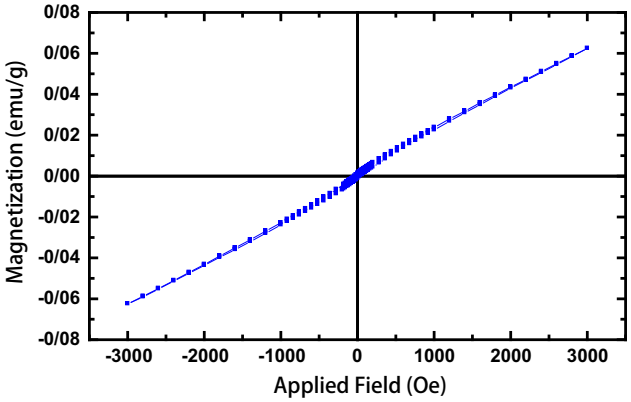

Fig. 4 VSM curves of Fe_2TiO_5 nanoparticles calcined at 700 °C

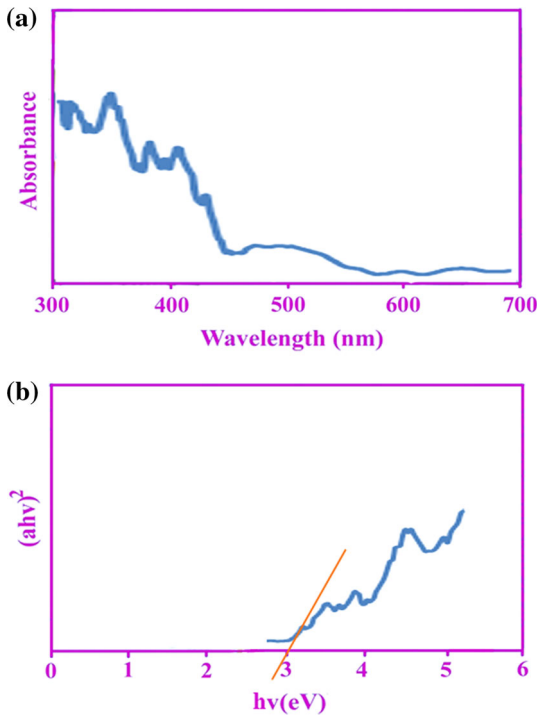

Fig. 5 **a** UV–vis absorption spectra of prepared Fe_2TiO_5 nanoparticles for 150 min at calcination temperature of 700 °C and **b** plot to determine the direct band gap of Fe_2TiO_5 nanoparticles

iron titanate obtained was studied by the degradation of methyl orange solution as a target pollutant. The photocatalytic degradation was performed with 150 mL solution of methyl orange (0.0005 g) containing 0.05 g of Fe_2TiO_5. This mixture was aerated for 30 min to reach adsorption equilibrium. Later, the mixture was placed inside the photoreactor in which the vessel was 15 cm away from the visible source of 400 W mercury lamps. The photocatalytic test was performed at room temperature. Aliquots of the mixture were taken at definite interval of times during the irradiation, and after centrifugation they were analyzed by

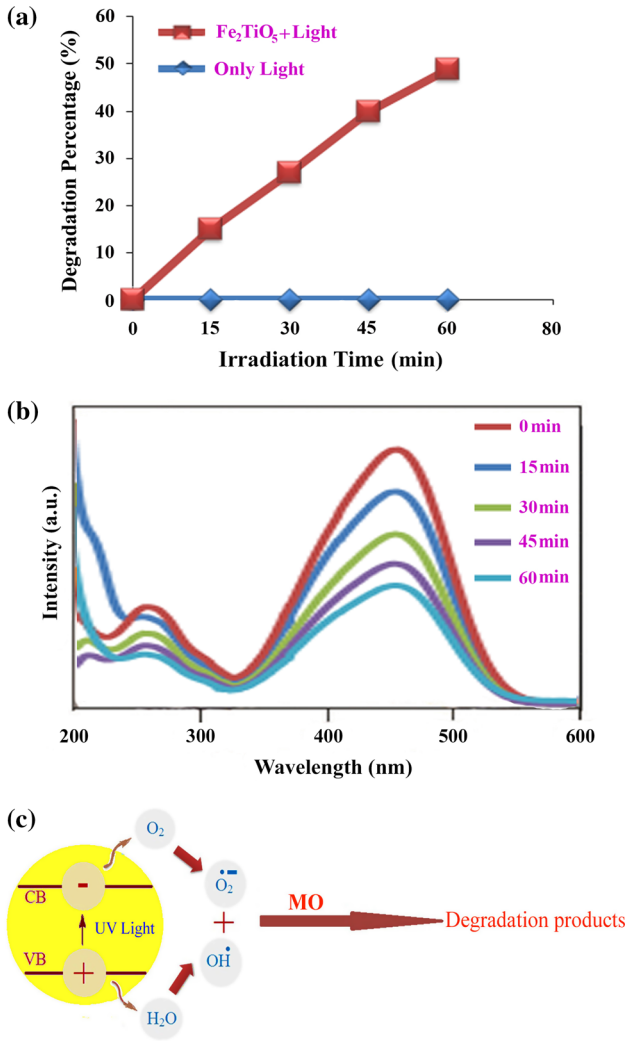

Fig. 6 **a** Photocatalytic methyl orange degradation of Fe_2TiO_5 nanoparticles under ultraviolet light, **b** fluorescence spectral time scan of methyl orange illuminated at 510 nm with Fe_2TiO_5 nanoparticles and **c** reaction mechanism of methyl orange photodegradation over Fe_2TiO_5 nanoparticles under ultraviolet light irradiation

a UV–vis spectrometer. The methyl orange (MO) degradation percentage was calculated as:

$$\text{Degradation rate } (\%) = \frac{A_0 - A}{A_0} \times 100$$

where A_0 and A are the absorbance value of solution at A_0 and A min, respectively.

3 Results and discussion

The XRD pattern of as-prepared Fe_2TiO_5 nanoparticles is shown in Fig. 1. Based on the Fig. 1, the diffraction peaks can be indexed to pure tetragonal phase of Fe_2TiO_5 (space group of Bbmm63 and JCPDS No. 09-0182). No other crystalline phases were detected. From XRD data, the crystallite diameter (D_c) of Fe_2TiO_5 nanoparticles was calculated to be 40 nm using the Scherer equation:

$$D_c = K\lambda/\beta\cos\theta$$

where β is the breadth of the observed diffraction line at its half intensity maximum (400), K is the so-called shape factor, which usually takes a value of about 0.9, and λ is the wavelength of X-ray source used in XRD. The morphology of the nanoparticles was investigated using SEM which demonstrates uniform nanoparticles with spherical shape homogenously distributed all over the sample, as it could be clearly observed in Fig. 2. The Fe_2TiO_5 nanoparticles with particle size of about 50–55 nm were observed. The EDS analysis measurement was used to investigate the chemical composition and purity of Fe_2TiO_5 nanoparticles. According to the Fig. 3, the product consists of Fe, Ti, and O elements. Furthermore, neither N nor C signals were detected in the EDS spectrum, which means the product is pure and free of any surfactant or impurity. The VSM magnetic measurements for the iron titanium oxide (Fig. 4) show the magnetic properties of nanoparticles calcined at 700 °C. The synthesized Fe_2TiO_5 indicates a paramagnetic behavior, a saturation magnetization of ~ 0.06 emug^{-1} was determined for the Fe_2TiO_5 nanoparticles. The room temperature UV–vis absorption spectra of Fe_2TiO_5 nanoparticles were also measured in the range of 300–700 nm. Figure 5a shows the diffuse reflection absorption spectra of the Fe_2TiO_5 nanoparticles calcinled at 700 °C. The figure indicates that the Fe_2TiO_5 nanoparticles shows absorption maxima at 365 nm, the direct optical band gap estimated from the absorption spectra for the Fe_2TiO_5 nanoparticles is shown in Fig. 5b. An optical band gap is obtained by plotting $(\alpha h\nu)^2$ versus $h\nu$ where α is the absorption coefficient and $h\nu$ is photon energy. Extrapolation of the linear portion at $(\alpha h\nu)^2 = 0$ gives the band gaps of 3 eV for perovskite Fe_2TiO_5 material. Photodegradation of methyl orange under UV light irradiation (Fig. 6a–c) was employed to evaluate the photocatalytic activity of the as-synthesized Fe_2TiO_5. No methyl orange was practically broken down after 60 min without using UV light irradiation or nanocrystalline Fe_2TiO_5. This observation indicated that the contribution of self-degradation was insignificant. The probable mechanism of the photocatalytic degradation of methyl orange can be summarized as follows:

$$Fe_2TiO_5 + h\nu \rightarrow Fe_2TiO_5^{\cdot} + e^- + h^+ \quad (1)$$

$$h^+ + H_2O \rightarrow OH^{\cdot} \quad (2)$$

$$e^- + O_2 \rightarrow O_2^{\cdot -} \quad (3)$$

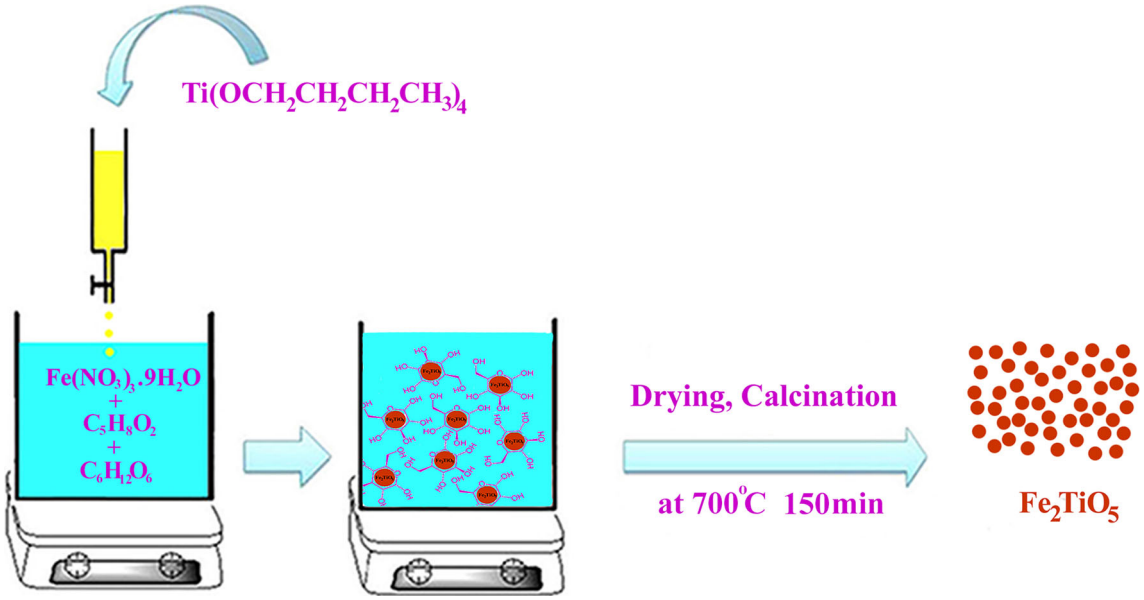

Scheme 1 Schematic diagram illustrating the formation of Fe_2TiO_5 nanoparticles

$$OH^{\cdot} + O_2^{\cdot -} + \text{ methyl orange} \rightarrow \text{Degradation products} \quad (4)$$

Using photocatalytic calculations by Eq. (1), the methyl orange degradation was about 50 % after 60 min irradiation of UV light, and nanocrystalline Fe_2TiO_5 presented high photocatalytic activity (Fig. 6a). The spectrofluorimetric time-scans of methyl orange solution illuminated at 510 nm with nanocrystalline Fe_2TiO_5 are depicted in Fig. 6b. Figure 6b shows continuous removal of methyl orange on the Fe_2TiO_5 under UV light irradiation. It is generally accepted that the heterogeneous photocatalytic processes comprise various steps (diffusion, adsorption, reaction, and etc.), and suitable distribution of the pore in the catalyst surface is effective and useful to diffusion of reactants and products, which prefer the photocatalytic reaction. In this investigation, the enhanced photocatalytic activity can be related to appropriate distribution of the pore in the nanocrystalline Fe_2TiO_5 surface, high hydroxyl amount and high separation rate of charge carriers (Fig. 6c). Furthermore, this route is facile to operate and very suitable for industrial production of Fe_2TiO_5 nanoparticles. In addition, this process can be versatile to easily synthesize other titanium based perovskite oxides. The synthesis pathway of Fe_2TiO_5 nanoparticles is shown in Scheme 1.

4 Conclusion

In this work, iron titanate nanoparticles were successfully synthesized by a novel sol–gel method at 700 °C for 150 min. The stages of the formation of Fe_2TiO_5, as well as the characterization of the resulting compounds were done using X-ray diffraction and energy dispersive X-ray spectroscopy. The products were analyzed by scanning electron microscopy (SEM), and ultraviolet–visible (UV–Vis) spectroscopy to be round, about 50–55 nm in size and Eg = 3 eV. When as prepared nanocrystalline iron titanate oxide was utilized as photocatalyst, the percentage of methyl orange degradation was about 50 % after 60 min irradiation of UV light.

Acknowledgments Authors are grateful to council of University of Borujerd Branch for providing financial support to undertake this work.

References

1. S. Khademolhoseini, M. Zakeri, S. Rahnamaeiyan, M. Nasiri, R. Talebi, J. Mater. Sci.: Mater. Electron. **26**, 7303 (2015)
2. P. Bakhshaei, A. Ataie, H. Abdizadeh, J. Nanostruct. **3**, 403 (2013)
3. R. Raeisi Shahraki, M. Ebrahimi, J. Nanostruct. **2**, 413 (2013)
4. M. Shakib Nahad, G. Mohammadi Ziarani, A. Badiei, A. Bananc, J. Nanostruct. **3**, 395 (2013)
5. M. Rahimi-Nasarabadi, J. Nanostruct. **4**, 211 (2014)
6. M. Najafi, H. Haratizadeh, M. Ghezellou, J. Nanostruct. **5**, 129 (2015)
7. M. Ahmadzadeh, M. Almasi-Kashia, A. Ramazani, J. Nanostruct. **5**, 97 (2015)
8. F.S. Ghoreishi, V. Ahmadi, M. Samadpourc, J. Nanostruct. **3**, 453 (2013)
9. C. Adán, J. Carbajo, A. Bahamonde, Catal. Today **143**, 247 (2009)
10. Z.Q. Liu, Y.C. Wang, W. Chu, J. Alloys Compd. **501**, 54 (2010)
11. R.S. Singh, T.H. Ansari, R.A. Singh, B.M. Wanklyn, B.E. Watt, Solid State Commun. **94**, 1003 (1995)

12. J.K. Srivastava, J. Hammann, K. Asai, K. Katsumata, Phys. Lett. **149**, 485 (1990)
13. J.L. Tholence, Y. Yeshurun, B. Wanlyn, Solid State Phys. **19**, 235 (1986)
14. K. Iwauchi, Y. Ikeda, Phys. Status Solidi **119**, K71 (1990)
15. S.W. Paulik, M.H. Zimerman, K.T. Faber, E.R. Fuller, J. Mater. Res. **11**, 2795 (1996)
16. E. Gunner, A.D. Petton, E. Woermann, A. Ender, Ber. Bun. Phys. Chem. **100**, 1839 (1996)
17. G.S. Ginley, M.A. Butler, J. Appl. Phys. **48**, 2019 (1977)
18. W. Waslaluddin, D.G. Syarif, J. Aust. Ceram. Soc. **49**, 141 (2013)
19. M.H. Zimmermann, K.T. Faber, E.R. Fuller, K.L. Kruger, K.J. Bowman, J. Am. Ceram. Soc. **79**, 1389 (1996)
20. J.K. Srivastava, J. Phys. Chem. Solids **49**, 115 (1988)
21. M.A. Madare, S.V. Salvi, Turk. J. Phys. **29**, 25 (2005)
22. N.M.L. Morais, P.C. Ske, R. Neto, Solid State Commun. **52**, 781 (1984)
23. A. Rahdar, M. Aliahmad, Y. Azizi, J. Nanostruct. **5**, 145 (2015)
24. M. Riazian, J. Nanostruct. **4**, 433 (2014)
25. L. Nejati-Moghadam, A. Esmaeili Bafghi-Karimabad, M. Salavati-Niasari, H. Safardoust, J. Nanostruct. **5**, 47 (2015)